Journal of Solid State Chemistry 261 (2018) 53–61

Contents lists available at ScienceDirect

Journal of Solid State Chemistry

journal homepage: www.elsevier.com/locate/jssc

Competitive adsorption of Pb(II), Cu(II), and Zn(II) ions onto hydroxyapatite-biochar nanocomposite in aqueous solutions

Yu-Ying Wang[a,b], Yu-Xue Liu[a,b], Hao-Hao Lu[a,b], Rui-Qin Yang[c,d], Sheng-Mao Yang[a,b,*]

[a] Institute of Environment, Resource, Soil, and Fertilizer, Zhejiang Academy of Agricultural Sciences, Hangzhou 310021, PR China
[b] Engineering Research Center of Biochar of Zhejiang Province, Hangzhou 310021, PR China
[c] Zhejiang Provincial Collaborative Innovation Center of Agricultural Biological Resources Biochemical Manufacturing, Zhejiang University of Science and Technology, Hangzhou 310023, PR China
[d] Zhejiang Provincial Key Lab for Chem & Bio Processing Technology of Farm Product, Zhejiang University of Science and Technology, Hangzhou 310023, PR China

ARTICLE INFO

Keywords:
Biochar
Hydroxyapatite
Nanocomposite
Competitive adsorption
Heavy metal

ABSTRACT

A hydroxyapatite-biochar nanocomposite (HAP-BC) was successfully fabricated and its physicochemical properties characterized. The analyses showed that HAP nanoparticles were successfully loaded on the biochar surface. The adsorption of Pb(II), Cu(II), and Zn(II) by HAP-BC was systematically studied in single and ternary metal systems. The results demonstrated that pH affects the adsorption of heavy metals onto HAP-BC. Regarding the adsorption kinetics, the pseudo-second-order model showed the best fit for all three heavy metal ions on HAP-BC. In both single and ternary metal ion systems, the adsorption isotherm of Pb(II) by HAP-BC followed Langmuir model, while those of Cu(II) and Zn(II) fitted well with Freundlich model. The maximum adsorption capacity for each tested metal by HAP-BC was higher than that of pristine rice straw biochar (especially for Pb(II)) or those of other reported adsorbents. Therefore, HAP-BC could explore as a new material for future application in heavy metal removal.

1. Introduction

Recently, heavy metals in water have become a worldwide problem, because most of them are toxic to organisms and accumulate in biota. In particular, Cd, Cu, Pb, and Zn cause cancers and damage the immune system [1–3]. Unlike other inorganic and organic pollutants, heavy metals are non-degradable and therefore persistent. Moreover, multiple heavy metals often coexist in contaminated water [4,5] due to a common geological source or co-disposal in the wastewater [6]. For instance, Zn and Pb are simultaneously discharged into the environment during the mining and milling of copper [7]. The coexistence of heavy metal pollutants in wastewater and contaminated soil means that their competitive sorption as well as their mobilities in the presence of each other should be studied [8]. Several methodes (adsorption, ion exchange, chemical precipitation, etc.) have been applied to remove these heavy metals from the environment [9–11]. While many of them have drawbacks (e.g., excessive time required, high costs, low efficiency, and high energy consumption), the adsorption process for aqueous effluents has become very attractive from the economic point of view [12,13]. Activated carbon, silica gels, iron oxide, carbonaceous nanofibers, zeolite, and attapulgite are among the conventional absorbent materials [13,14]. However, they have some disadvantages including tendencies for oxidation and aggregation, limited adsorption capacity, high cost, and low selectivity [15]. Therefore, developing multi-functional adsorbents is considered critical for treating heavy metal pollution.

Nowadays, biochar (biomass-derived black carbon) has attracted attention as a new adsorbent. It is carbon-rich and pyrolyzed in a closed container under anaerobic condition [16]. Because of its especial properties (e.g., high surface area and cation exchange capacity), biochar can be used for soil improvement, fertility enhancement, and carbon sequestration, etc. [17,18]. Moreover, biochar based on agricultural and forestry by-products could potentially replace activated carbons as an economical adsorbent for contaminants. However, the as-prepared biochars usually have a relatively low adsorption capacity for heavy metals [19]. Several methods have thus been developed to modify biochars. In particular, surface modifications such as loading nanoparticles to prepare biochar nanocomposites can remarkably improve the removal ability for various water pollutants [20–22].

Hydroxyapatite [HAP, $Ca_{10}(PO_4)_6(OH)_2$] is found naturally in human bones and teeth. It is usually applied as hard tissue implants and carriers of genes, enzymes, and proteins [23,24]. Hydroxyapatite is

* Corresponding author at: Institute of Environment, Resource, Soil, and Fertilizer, Zhejiang Academy of Agricultural Sciences, Hangzhou 310021, PR China.
E-mail address: yangshengmao@263.net (S.-M. Yang).

https://doi.org/10.1016/j.jssc.2018.02.010
Received 20 December 2017; Received in revised form 9 February 2018; Accepted 12 February 2018
Available online 15 February 2018
0022-4596/

also particularly well-suited for immobilizing metallic cations on several sites of P-OH groups on its surface. Being environmentally friendly, HAP-based adsorbents can be safely used in natural water [25]. However, because of the high surface energy caused by van der Waals forces, HAP nanoparticles tend to form aggregates in aqueous solutions., dramatically decreasing their surface area and removal performance. Therefore, compositing hydroxyapatite with biochar may produce desirable adsorption properties that cannot be achieved by either component alone.

The objective of this work was to fabricate hydroxyapatite-biochar nanocomposite wtih the advantages of both biochar and hydroxyapatite nanoparticles for removing Pb(II), Cu(II), and Zn(II). The hydroxyapatite-biochar (HAP-BC) nanocomposite was carefully characterized. The adsorption behaviors of single and ternary metal solutions on HAP-BC nanocomposite were also investigated. The unmodified biochar derived from rice straw was used as a comparison. The influences of pH, contact time, initial ion concentration, ionic strength, and other coexisting ions on the performance were studied. Langmuir and Freundlich adsorption isotherm models, and different kinetic equations were applied to calculate the isotherm parameters and study the adsorption kinetics, respectively. In addition, the mechanisms for heavy metal removal by modified and unmodified biochars were explained.

2. Materials and methods

2.1. Materials

The chemicals used in the experiments, including NaCl, KCl, $MgCl_2 \cdot 6H_2O$, $CaCl_2$, $(NH_4)_2HPO_4$, HCl, NaOH, $Cu(NO_3)_2 \cdot 3H_2O$, $Pb(NO_3)_2$, and $Zn(NO_3)_2 \cdot 6H_2O$, being commercially available and of analytical grade, were purchased from Sinopharm Chemical Reagent Co., Ltd. Deionized water was used in all experiments.

2.2. Preparation of biochar

The biochar prepared in this study was derived from rice straw through a typical slow pyrolysis process [26]. The rice straw came from the Yangdu experimental baseof Zhejiang Academy of Agricultural Sciences. Firstly, rice straw was put in a programmable tube furnace (Hangzhou Lan Tian Instrument Co., LTD) and pyrolyzed under anaerobic conditions at 500 °C for 3 h with the heating rate of 25 °C min^{-1}. Then, the sample was cooled to room temperature naturally to obtain the pristine biochar (BC). The HAP-BC nanocomposite was prepared as follows. $CaCl_2$ (1.11 g, 0.1 M) was first dissolved in 100 mL of deionized water with vigorous stirring, to which 1 g of the prepared BC was added to form a suspension solution A. $(NH_4)_2HPO_4$ (0.792 g, 0.06 M) was then dissolved in 100 mL of deionized water with vigorous stirring to form solution B. The solutions A and B were both adjusted to pH = 10.0 using 0.1 M HCl or NaOH. Finally, solution B was added into A gradually. After 24 h of incubation, the precipitate was isolated by centrifugation and washed three times with anhydrous ethanol, and then dried overnight to obtain the HAP-BC nanocomposite.

2.3. Biochar characterization

SEM analysis was performed on a JSM-6700F field emission scanning electron microscope (FESEM). The biochar samples were coated with a thin film of gold to increase the conductivity. Elemental composition analysis of the biochars was conducted by Energy-dispersive X-ray spectroscopy (EDX). The XRD patterns were measured with a Bruker D8 Advance X-ray diffractometer. IR spectra of the biochars were obtained on a Nicolet iS10 FT-IR spectrometer in the range from 4000–400 cm^{-1}. The specific surface area was measured by a Nova 2000e surface area analyzer (Quantachrome, USA). The zeta potential was obtained using a particle analyzer (Nano ZS90).

2.4. Sorption experiments

The standard stock solutions of Pb(II), Cu(II), and Zn(II) ions (each of 1000 mg L^{-1}) were prepared with $Pb(NO_3)_2$, $Cu(NO_3)_2 \cdot 3H_2O$, and $Zn(NO_3)_2 \cdot 6H_2O$, respectively. The adsorption experiments were conducted by mixing biochar (50 mg) with the heavy metal solution (50 mL) at 25 °C. The influence of pH on the adsorption ability of biochars was examined for pH = 2–6. The pH of the solution was controlled by HCl and/or NaOH. To measure the sorption kinetics, the adsorption on biochars was examined at different time intervals (10, 30, 60, 180, 300, 480, 720, and 1440 min). Different initial concentrations of the heavy metals (25, 50, 100, 200, 300, 500, 800, and 1000 mg L^{-1}) were applied to obtain the sorption isotherms. In addition, the influence of ionic strength on the competitive adsorption was also studied, by adjusting the ionic strengths of the solution to 0, 0.001, 0.005, 0.01, 0.05, 0.1 and 0.5 M using NaCl. The effects of four common coexisting cations, Na(I), K(I), Ca(II), and Mg(II), were also studied by adding 0.01 M of NaCl, KCl, $CaCl_2$, or $MgCl_2 \cdot 6H_2O$ to 50 mg L^{-1} heavy metal solutions, respectively.

At the end of each experiment, the mixture was filtered and the concentration of residual heavy metal ions in the filtrate was determined by inductively coupled plasma–atomic emission spectroscopy (ICP-AES, Prodigy). All adsorption studies were repeated in triplicate, and the averaged values were given. The adsorption efficiency (q_e) and uptake percentage (U%) were calculated as follows:

$$q_e = \frac{(C_0 - C_e)V}{W}$$

$$U\% = \frac{(C_0 - C_e)100\%}{C_0}$$

where C_0 and C_e ($mg \cdot L^{-1}$) are the initial and equilibrium concentrations of the heavy metal, respectively, V (mL) is the total volume of the solution, and W (mg) is the weight of the biochar.

2.5. Regeneration of the sorbent

First, 0.05 g of HAP-BC was added to 50.0 mL of 50 mg L^{-1} mixed heavy metal solutions, buffered at optimum pH, and stirred for 24 h. After reaching adsorption equilibrium in the ternary metal system, the metal-loaded HAP-BC was removed and placed in 50 mL of 0.2 M HCl and shaken in an oscillator for 30 min. Afterwards, HAP-BC was collected by centrifugation, washed, and dried for the next cycle. This process was repeated for five cycles.

3. Results and discussion

3.1. Biochar characterization findings

The XRD patterns of BC and HAP-BC were shown in Fig. 1a. The peaks for BC at 28° and 41° confirmed the presence of sylvite (KCl), while those at 29.5° and 31° were attributed to $CaMg(CO_3)_2$/dolomite [27]. The XRD pattern of HAP-BC was significantly different: all the diffraction peaks can be indexed as hydroxyapatite with the lattice parameters a = 9.423 Å, c = 6.883 Å, and space group $P6_3/m$ (JCPDS 89–6440), indicating that HAP was loaded on the surface of biochar. The average crystalline size calculated by Scherrer's formula was 3.85 nm. The FT-IR spectra of the two samples are shown in Fig. 1b. In the spectrum for BC, the broad band centered at 3445 cm^{-1} (between 3000 and 3500 cm^{-1}) can be assigned to –OH stretching vibrations of water [28]. The peak at 1093 cm^{-1} was assigned to C–O stretching of the $-OCH_3$ group, and that at 1434 cm^{-1} was assigned to $-CH_2-$ groups [29]. The band at 1601 cm^{-1} represented C=O stretching vibrations, whereas those at 2357 cm^{-1} could be assigned to the O=C=O stretching vibrations [29]. These organic functional groups may be attributed to the lignin structure in rice straw. The vibration peaks of

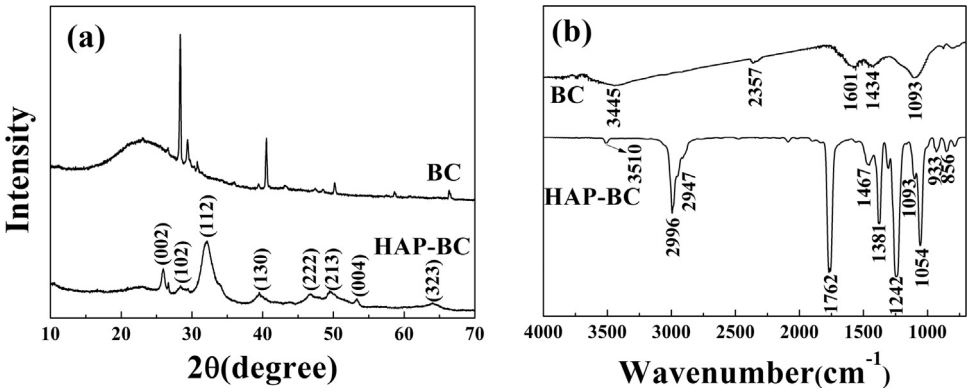

Fig. 1. (a) XRD patterns and (b) FT-IR spectra of BC and HAP-BC.

HAP-BC were similar to those of HAP reported in the literature, with a series of strong bands in the range of 920–1200 cm^{-1} due to various vibrations of $-PO_4^{3-}$ [30,31]. The peak at 933 cm^{-1} was due to the bending vibration of the P–O bond, and the symmetric sorption band at 1054 cm^{-1} was assigned to PO_4^{3-}. Moreover, the peak at 1467 cm^{-1} was due to the stretching vibration of CO_3^{2-} or –COO, while that at 3510 cm^{-1} was due to the –OH stretching. HAP-BC also had several additional peaks at 2996 and 2947 cm^{-1} (C–H of methylene), 1093 cm^{-1} (C–O), as well as 880–828 cm^{-1} (possibly the band of C–Cl or C–H). Thus, the XRD and FT-IR results indicate that HAP was successfully loaded onto the BC. The presence of these functional groups can facilitate the complexation and precipitation of heavy metal ions.

The morphology and size of BC and HAP-BC particles were characterized by FESEM, and representative images are shown in Fig. 2. In the panoramic image (Fig. 2a), BC derived from rice straw appeared in the form of irregular sheets, and the heterogeneous grain size corresponds to the typical microstructure of BC. The corresponding EDX analysis (Fig. 2b) suggested the BC sample contained carbon, oxygen, a small amount of potassium, plus gold and copper that were introduced during the SEM sample preparation. The morphology of HAP-BC was significantly different, since the FESEM image shows the presence of many HAP nanoparticles on the surface of the BC sheets (Fig. 2c). The high-magnification image (Fig. 2c, inset) unambiguously reveals that the HAP nanoparticles were homogeneously grown on the surface of biochar. According to the EDX analysis (Fig. 2d), these nanoparticles contained calcium, phosphorus, oxygen, carbon, copper, and gold. Carbon came from biochar; calcium, phosphorus, and oxygen from HAP; and copper and gold from the sample preparation procedure. Taken together, the results from XRD, FT-IR, and FESEM analyses confirmed that the HAP-BC nanocomposite was prepared successfully in this work.

In addition, the specific surface area and pore volume of BC and HAP-BC were measured. The isotherm of BC (Fig. 3a) was that of type IV with a type H3 hysteresis loop, suggesting mesoporous structures. The hysteresis loop was mainly present in the range of 0.4–1.0 P/P_o,

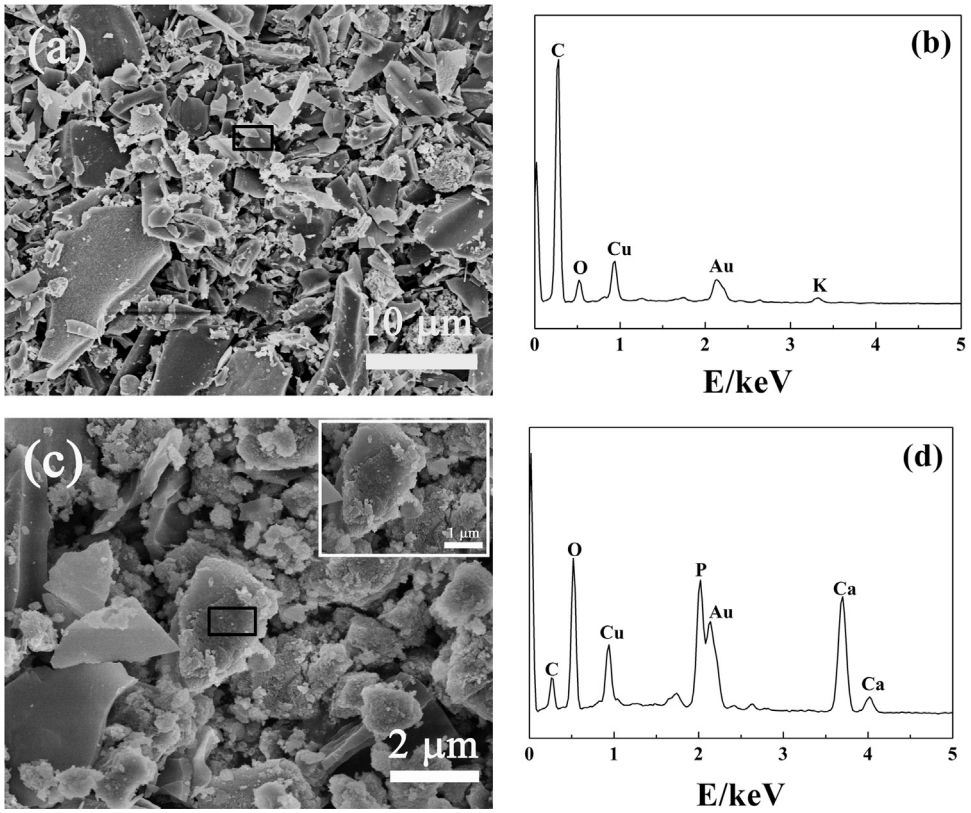

Fig. 2. (a and c) FESEM images and (b and d) EDX spectra of BC (a and b) and HAP-BC (c and d).

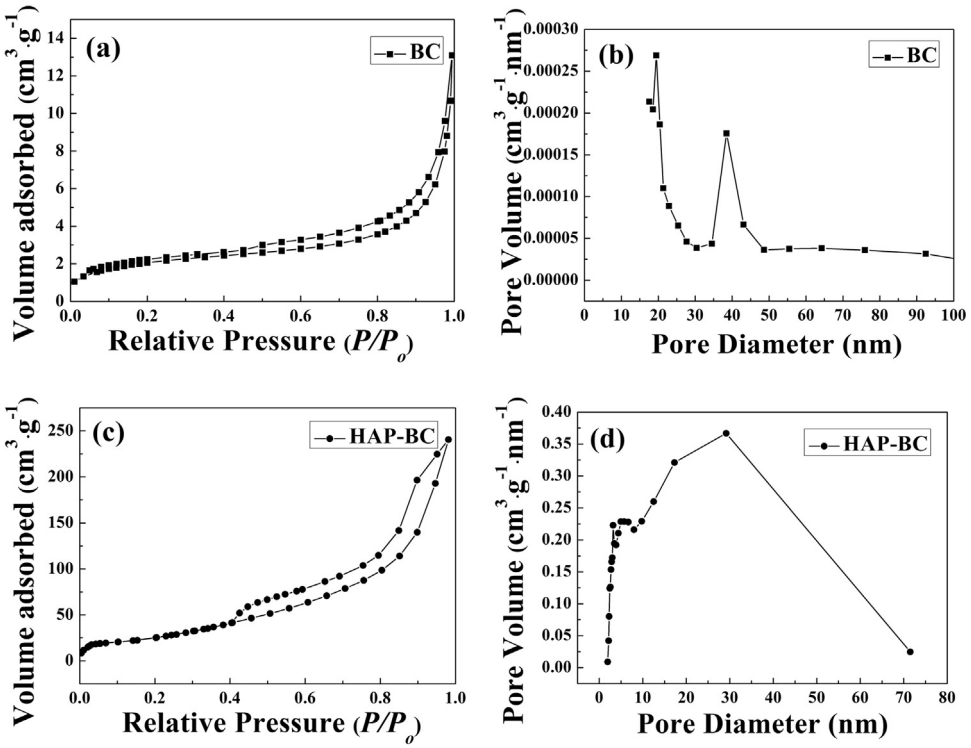

Fig. 3. (a and c) Nitrogen adsorption-desorption isotherms and (b and d) pore size distributions of BC (a and b) and HAP-BC (c and d).

demonstrating that the structures were mesopores. In contrast, the isotherm of HAP-BC (Fig. 3c) is a combination of types I and IV [24,32]. The high adsorption at low relative pressures ($P/P_0 < 0.2$) means that the microporous structure was present in HAP-BC (type I) [33]. Between $P/P_o = 0.4$ and 1.0, HAP-BC displayed a type H3 hysteresis loop [34], which belongs to the mesoporous assembled by HAP nanoparticles. The BET surface area, pore diameter (d), and total pore volume (V_{total}) of HAP-BC were 126.41 $m^2\ g^{-1}$, 9.76 nm, and 0.309 $cm^3\ g^{-1}$; whilst those of BC were 7.15 $m^2\ g^{-1}$, 11.34 nm, and 0.020 $cm^3\ g^{-1}$, respectively. The significant increases in BET surface area and total pore volume of HAP-BC are expected to benefit the heavy metal adsorption process. Moreover, the pore size distribution (Fig. 3b and d) had peaks centered at 19.7 and 38.2 nm for BC, and 4.6 and 29.2 nm for HAP-BC. The HAP-BC with a high surface area is beneficial for water treatment or other environmental remediation applications.

3.2. Adsorption isotherms of single ionic species

The effect of the initial concentration of single Pb(II), Cu(II), or Zn(II) ions on their removal was investigated. From Figs S1a and S1b, the adsorption efficiency q_e increased with the initial ionic concentration for both BC and HAP-BC, with the latter displaying relatively higher adsorption capacity for each of the ions.

The Langmuir and Freundlich isotherm models were applied to interpret the adsorption data [35,36]. The linear form of the Langmuir isotherm is as follows

$$\frac{C_e}{q_e} = \frac{1}{q_{max} K_L} + \frac{C_e}{q_{max}}$$

where q_e and C_e are respectively the equilibrium adsorbed amount (mg/g) and the equilibrium metal ion concentration in solution (mg/L). K_L (L/mg) is the Langmuir constant, and q_{max} (mg/g) is the maximum adsorption capacity. The linearized Freundlich model is

$$\mathrm{Ln}q_e = \mathrm{Ln}K_F + \frac{1}{n}\mathrm{Ln}C_e$$

where K_F is the adsorption capacity (mg/g) and n is the adsorption intensity.

Fig. S2 depicts linear plots comparing the isotherm models for single ions, and the calculated Langmuir and Freundlich constants are given in Table S1. For both BC and HAP-BC, the Langmuir isotherm fits the Pb(II) data well with high correlation coefficients. In contrast, the experimental data for Cu(II) and Zn(II) correlate better with the Freundlich model (Fig. S2). The maximum adsorption values for Pb(II), Cu(II), and Zn(II) were 561.80, 826.45, and 925.93 mg/g by BC; and about 1000, 833.33, and 935.93 mg/g by HAP-BC, respectively. Therefore, the adsorption of Pb(II) onto both BC and HAP-BC obeyed the Langmuir model (i.e., mainly monolayer adsorption), while that of Cu(II) and Zn(II) fitted the Freundlich model (i.e., multilayer adsorption on the heterogeneous biochar surface). The maximum adsorption capacity for the tested heavy metals is generally higher by HAP-BC than by BC, especially for Pb(II).

3.3. Sorption of ternary metal solutions on BC and HAP-BC

3.3.1. Effect of pH

The effects of initial pH (2.0–6.0) on the competitive adsorption of Pb(II), Cu(II), and Zn(II) ions by BC and HAP-BC are shown in Fig. 4a and b, respectively. Apparently, pH plays a vital role in many multi-species adsorptions as reported in other literatures [27,37]. When the pH is increased from 2.0 to 3.0, there is an increase in the removal percentages. At low pH (pH = 2), the removal capacities for all heavy metal ions are low, and then they sharply increase with the pH value. This increase of heavy metal removal at higher pH values can be attributed to the decrease of adsorption competition from protons. When the pH is higher, the positive charge on the biochar surface would decrease, leading to a decline of the electrostatic repulsion between the heavy metals and the biochar surface [37]. Above pH 5.0, the adsorption capacity was almost unchanged, which could be further confirmed by the biochar's point of zero charge (pH_{pzc}) and zeta potential. The value of the zeta potential is related to the pH-dependent surface charge of biochars, and will reflect their adsorption properties

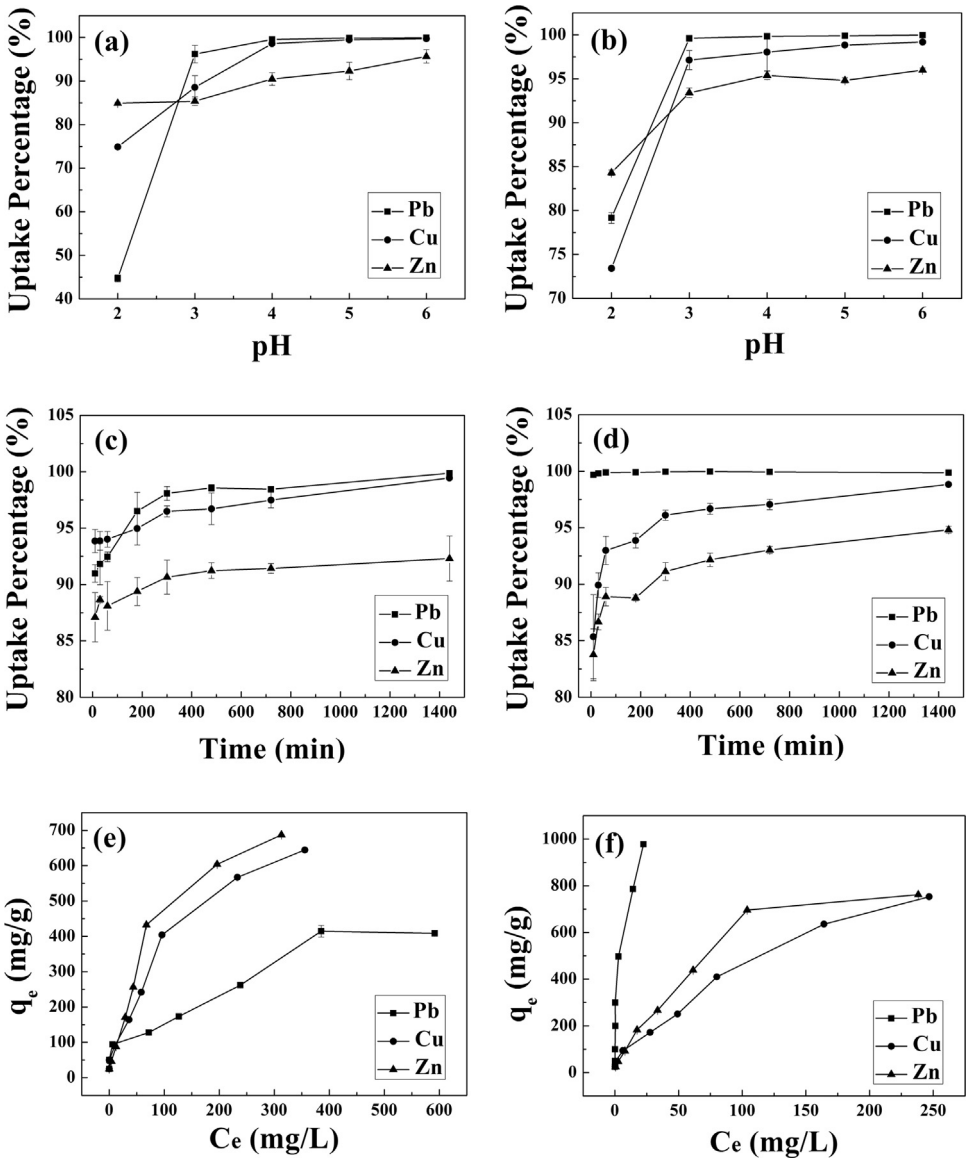

Fig. 4. Effect of pH on the removal of Pb(II), Cu(II), and Zn(II) by (a) BC and (b) HAP-BC at room temperature for 24 h in the ternary system. Removal of Pb(II), Cu(II), and Zn(II) at pH 6.0 by (c) BC and (d) HAP-BC at room temperature in the ternary system, after different contact times.; Effect of initial heavy metal ion concentrations on the removal of Pb(II), Cu(II), and Zn(II) at pH 6.0 by (e) BC and (f) HAP-BC in the ternary system.

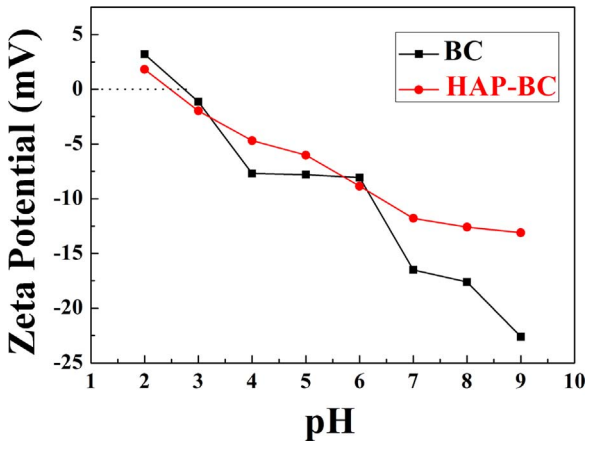

Fig. 5. Zeta potentials of BC and HAP-BC at different solution pH values.

[15,27]. The zeta potentials of BC and HAP-BC are shown in Fig. 5, with pH_{pzc} values of 2.7 and 2.5, respectively. When the pH is below pH_{pzc}, the biochar surface is positively charged, which does not favor the heavy metal adsorption due to electrostatic repulsion. When the solution pH is greater than pH_{pzc}, the surface of the biochars acquires a negative charge, leading to significant electrostatic attraction between the heavy metals and the positively charged surface. In our experiment, an increase occurred at pH 2.0–3.0, which is consistent with the zeta potential analysis results. The adsorption capacity for mixed Pb-Cu-Zn metal ions by either BC or HAP-BC was the highest at pH = 6 with the tested pH range. Therefore, pH = 6 was considered the optimum condition and used hereafter.

3.3.2. *Adsorption kinetics of ternary metal solutions*

The influence of contact time on the competitive adsorption of heavy metals by BC and HAP-BC is shown in Fig. 4c and d, respectively. As plotted in Fig. 4c, the adsorption rate was high during the first 5 h, in which the respective removal percentages of Pb(II), Cu(II), and

Table 1
Pseudo-first-order and pseudo-second-order kinetic parameters for Pb(II), Cu(II), and Zn(II) adsorbed by BC and HAP-BC in the ternary metal system.

Sample	Ion	Experimental parameters		Pseudo-first order			Pseudo-second order		
		pH	$q_{e,exp}$ (mg g^{-1})	k_1 (min^{-1})	$q_{e,cal}$ (mg g^{-1})	R^2	k_2 (g mg^{-1} min^{-1})	$q_{e,cal}$ (mg g^{-1})	R^2
BC	Pb(II)	5	49.95	0.0038	4.41	0.941	0.0041	49.98	0.999
BC	Cu(II)	5	49.80	0.0024	3.52	0.938	0.0032	49.70	0.999
BC	Zn(II)	5	46.20	0.0026	2.34	0.979	0.0057	46.17	0.999
HAP-BC	Pb(II)	5	49.99	5.27×10^{-4}	22.17	−0.0751	0.23	49.95	0.999
HAP-BC	Cu(II)	5	49.50	0.0027	4.62	0.950	0.0031	49.46	0.999
HAP-BC	Zn(II)	5	47.50	0.0026	4.80	0.973	0.0027	47.46	0.999

Zn(II) were 98.1%, 96.5%, and 90.7%. Then, the adsorption rate decreased, and the adsorption equilibrium was achieved after 8 h. For HAP-BC, the removal of Pb(II) was much faster (nearly complete within 10 min), indicating a high removal efficiency. For both Cu(II) and Zn(II), the adsorption rate was very high during the first 1 h and then became slow, and the adsorption equilibrium was gradually achieved within 8 h. Furthermore, in both cases, the uptake efficiency of Pb(II), Cu(II), and Zn(II) by HAP-BC was higher than that by BC.

To further understand the competitive adsorption behaviors of Pb(II), Cu(II), and Zn(II), the adsorption kinetics in mixed solutions were analyzed by fitting with different kinetic models, in the same way as for single-species adsorption [38,39]. The pseudo-first-order and pseudo-second-order kinetic equations can be described as follows (in this order):

$$\log(q_e - q_t) = \log q_e - \frac{tk_1}{2.303}$$

$$\frac{t}{q_t} = \frac{1}{k_2 q_e^2} + \frac{t}{q_e}$$

where q_e and q_t (mg g^{-1}) represent the amounts of adsorption at equilibrium and time t, and k_1 (min^{-1}) and k_2 (g mg^{-1} min^{-1}) are the pseudo-first-order and pseudo-second-order reaction rate constants, respectively.

The experimental kinetic data were fitted with both kinetic equations (Fig. S3), and the obtained parameters and correlation coefficients are listed in Table 1. For both BC and HAP-BC, the experimental data could be better fitted with the pseudo-second-order kinetic model (R^2 = 0.999). Moreover, the theoretical $q_{e,cal}$ values for all three metal ions calculated from this model were very close to the experimental values ($q_{e,exp}$). Therefore, the adsorptions of mixed Pb(II), Cu(II), and Zn(II) were well represented by pseudo-second-order kinetics, indicating that the process involved chemisorption between metal ions and biochars [40,41].

To further understand the removal mechanism of these heavy metal ions by the two adsorbents, BC and HAP-BC loaded with metals were analyzed by XRD. According to the results in Fig. 6a, the pattern of metal-loaded BC shows a broad hump peak at 23°, indicating that the sample was amorphous [27]. Compared with Fig. 1a (BC before adsorption), the peaks of sylvite (KCl) and $CaMg(CO_3)_2$/dolomite disappeared, because these substances may dissolve in solution during the adsorption process. The XRD pattern of metal-loaded HAP-BC was quite different from that before adsorption (Fig. 1a), as the results indicate hexagonal pyromorphite ($Pb_5(PO_4)_3Cl$)), which has the lattice parameters a = 9.987 Å, c = 7.33 Å, and space group $P6_3/m(176)$ (JCPDS file 190701). The average crystalline size calculated by Scherrer's formula was 25.04 nm. Moreover, all the diffraction peaks are strong and sharp, suggesting that the pyromorphite was well crystallized. In the corresponding FESEM image (Fig. 6b), a large number of shuttle-shaped particles (presumably pyomorphite) and their assemblies were present on the surface of modified biochar. These results further confirm that the adsorption Pb(II) by HAP-BC was related to chemical precipitation, while that of Cu(II) and Zn(II) by HAP-BC, as well as that for all three metal ions by BC, was related to electrostatic interactions.

3.3.3. Adsorption isotherms in ternary metal solutions

The adsorption isotherms for ternary metal solution by BC and HAP-BC are shown in Fig. 4e and f. For BC, the adsorption capacities followed the order of Zn(II) > Cu(II) > Pb(II), while it was Pb(II) > Zn(II) > Cu(II) for HAP-BC. These results are consistent with the ordering for single ion adsorption. However, when we applied the above-mentioned isotherm models to the mixed Pb-Cu-Zn system (linear plots in Fig. S4, and the constants in Table 2), all three experimental adsorption isotherms by BC could be better fitted by the Freundlich model, which is different from the single ion systems. This suggests that the adsorption of the three co-existing ions on pristine biochar is a multilayer adsorption process. The maximum adsorption capacities by BC in the ternary metal system (438.60, 724.64, and 840.34 mg/g for Pb(II), Cu(II), and Zn(II), respectively) are lower than those in the single-ion systems. A different scenario was observed for HAP-BC: from Fig. S4c and S4d and Table 2, the Langmuir isotherms correlated better than the Freundlich ones with the experimental data for Pb(II), whereas the opposite occurred for

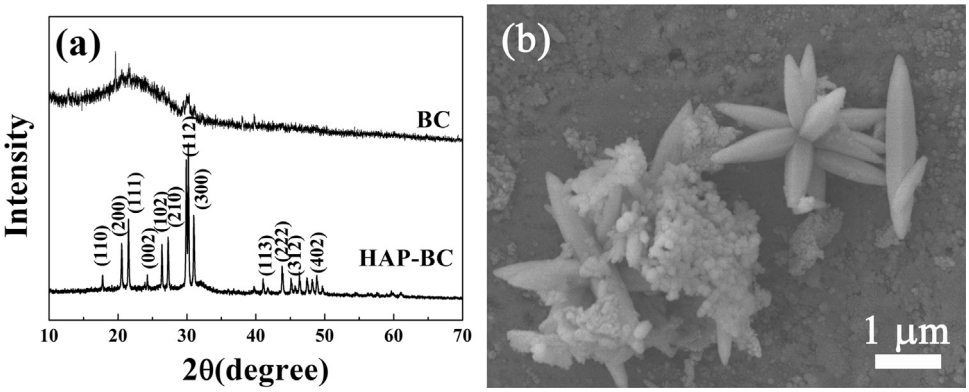

Fig. 6. (a) XRD patterns of BC and HAP-BC and (b) FESEM image of HAP-BC after treatment with the mixed Pb-Cu-Zn solution.

Table 2
Langmuir and Freundlich parameters for Pb(II), Cu(II), and Zn(II) adsorbed by BC and HAP-BC in the ternary system.

Sample	Ion	Langmuir constants			Freundlich constants		
		K_L (L mg^{-1})	q_{max} (mg g^{-1})	R^2	K_F (mg g^{-1}) (L mg^{-1})$^{1/n}$	n	R^2
BC	Pb(II)	0.013	438.60	0.847	73.92	4.38	0.911
BC	Cu(II)	0.016	724.64	0.876	55.35	2.56	0.933
BC	Zn(II)	0.013	840.34	0.899	39.70	2.08	0.909
HAP-BC	Pb(II)	0.85	961.54	0.977	283.96	2.21	0.920
HAP-BC	Cu(II)	0.017	854.70	0.780	54.19	2.26	0.964
HAP-BC	Zn(II)	0.016	980.39	0.914	31.62	1.63	0.980

Cu(II) and Zn(II). These results mean that Pb(II) likely formed monolayer coverage on both BC and HAP-BC, while Cu(II) and Zn(II) were adsorbed in multilayers. The Langmuir (K_L) and Freundlich (K_F) constants of Pb (II) on HAP-BC are higher than previously reported adsorbent [11], indicating the relatively higher removal capacities of HAP-BC. According to the Langmuir isotherm model, the adsorption capacities of HAP-BC (961.54, 854.70, and 980.39 mg/g for Pb(II), Cu(II), and Zn(II), respectively) are higher than those by BC, especially for Pb(II). For HAP-BC, these values in the ternary system are close to their counterpart in the single-ion systems.

Remarkably, the removal capacities of HAP-BC were higher than those previously reported for HAP and other adsorbents. For example, Ding et al. investigated the competitive sorption of Pb(II), Cu(II), and Ni(II) on uniform carbonaceous nanofibers, with the respective single-metal maximum sorption capacities being 795.65, 204.00, and 156.70 mg/g at pH 5.5 and 25 ℃ [14]. Saoiabi et al. used organophosphonate-modified HAP for Zn(II) and Pb(II) adsorption, with the highest capacities being 270 mg/g for Zn(II) and 454 mg/g for Pb(II) [25]. Jiang et al. found that the removal capacities for mixed Pb(II), Cu(II), and Cd(II) by hollow HAP were 99.794, 66.52, and 38.78 mg/g, respectively [24]. Chen et al. reported the adsorption capacities (q_m) were 35.5, 34.1, 10.2 mg/g for Cu(II), Pb(II), and Zn(II) when using the cross-linked chitosan with epichlorohydrin [42]. Zhu et al. examined a novel xanthate-modified magnetic chitosan adsorbent, and its respective maximum adsorption capacities for mixed Pb(II), Cu(II), and Zn(II) were 76.9, 34.5, and 20.8 mg/g [11]. Depci et al. investigated the competitive adsorption of Pb(II) and Zn(II) on activated carbon, and the measured adsorption amounts were 13.23 and 7.54 mg/g, respectively [43]. The HAP-BC nanocomposite prepared in this study achieved excellent adsorption performance that cannot be obtained by either of the components alone. Therefore, it could be an high-efficiency adsorbing material.

3.4. Effect of ionic strength

NaCl was used to adjust the solution at room temperature to ionic strengths of 0, 0.001, 0.005, 0.01, 0.05, 0.1, and 0.5 mol L^{-1}. Fig. 7a describes the effects of ionic strength on the removal of mixed heavy metals by HAP-BC. Apparently, the NaCl concentration had little or no effect on the removal of Pb(II), which can be attributed to the chemical precipitation mechanism, as mentioned above. The presence of NaCl did have a little influence on Cu(II) and Zn(II) removal capacities at low concentrations (0.001 and 0.005 mol L^{-1}). Nevertheless, these values were reduced slightly at higher NaCl concentrations (0.1 and 0.5 mol L^{-1}). Since Na(I) and Cl$^-$ are monovalent ions, at low concentrations they display no or slight competition with Cu(II) and Zn(II) [27]. At high concentrations, Na(I) and Cl$^-$ cause steric hindrance and also compete for surface adsorption sites on HAP-BC, leading to a reduced capacity for heavy metal adsorption.

3.5. Effect of other coexisting cations

Other metal ions existing in water will compete with heavy metals in the adsorption process. Thus, in this paper, we examined the effect of Na(I), K(I), Ca(II), and Mg(II) in water on the removal of mixed heavy metals by HAP-BC, and the result is shown in Fig. 7b. Apparently, the

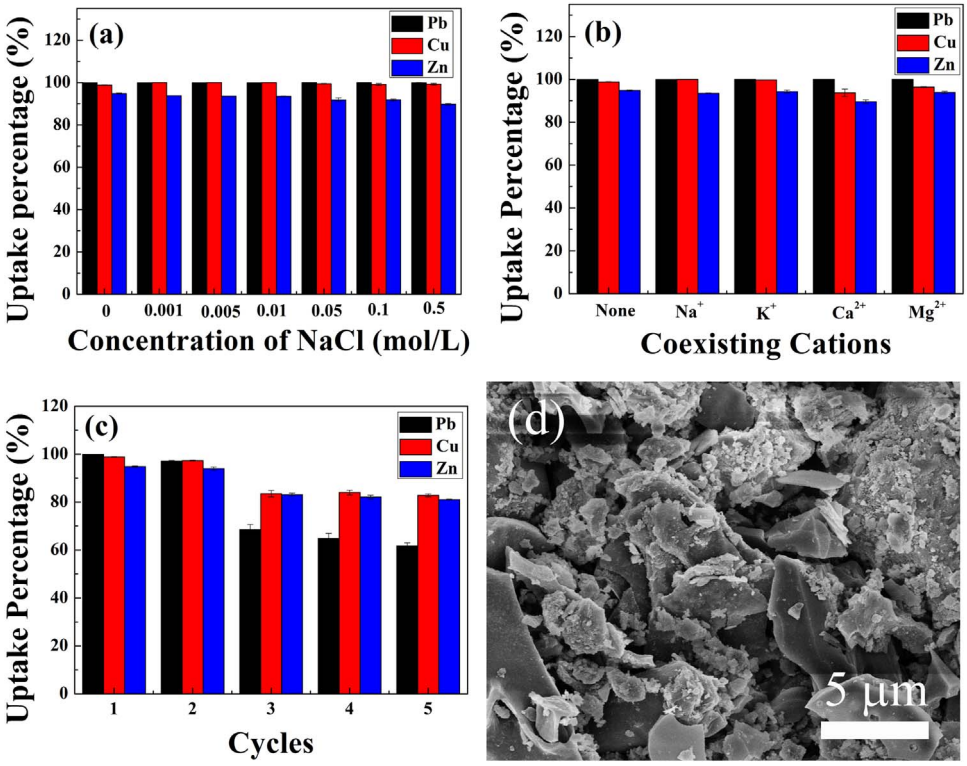

Fig. 7. (a) Effect of NaCl concentration on Pb(II), Cu(II), and Zn(II) removal by HAP-BC in the ternary system. (b) Effect of competing cations on Pb(II), Cu(II), and Zn(II) adsorption onto HAP-BC in the ternary system. (c) Uptake percentages of Pb(II), Cu(II), and Zn(II) in the mixed solution by HAP-BC over five consecutive adsorption–desorption cycles.

selectivities of HAP-BC towards each metal ion was only slightly affected by the presence of Na(I) and K(I), as their uptake percentage remained almost constant. In contrast, Ca(II) and Mg(II) reduced the Cu(II) and Zn(II) removal percentage more than the monovalent cation Na(I) and K(I) did (with the influence of Ca(II) stronger than that of Mg(II)), whereas they had no effect on Pb(II). This is because Mg(II) has a stronger covalent nature compared to Ca(II), hence Mg(II) ions display stronger hydration which reduces their interaction with the surface of HAP-BC [26,44]. Thus, compared with Ca(II), Mg(II) has a weaker competitive uptake over Cu(II) and Zn(II), but stronger than that of Na(I) and K(I).

3.6. Desorption studies

Desorption is important for the recovery of heavy metals adsorbed on the biochar surface, as well as for regenerating the adsorbent for reuse. In order to protonate the acid sites of HAP-BC to remove the heavy metals, HCl solution was used as the eluent. The adsorption/desorption cycles were repeated five times, as shown in Fig. 7d. The adsorption capacity decreased gradually with the cycles. For the first two cycles, it remained practically the same for all three ions. From the second to the third cycle, however, there was a decrease of 28.7%, 13.8%, and 11.0% in the amounts of adsorbed Pb(II), Cu(II), and Zn(II) ions, respectively. Nevertheless, the amount of each adsorbed heavy metal ion changed very little from the third cycle onward. In the fifth cycle, the uptake percentages of Pb(II), Cu(II), and Zn(II) were no less than 61%, 82%, and 81%, respectively. The decreasing adsorption capacity during the cycles could be attributed to the wastage of the adsorbent. Moreover, the morphology of the HAP-BC after recycling was characterized by FESEM. As shown in Fig. 7d, the morphology of HAP-BC after recycling did not change too much compared with that before adsorption (Fig. 2c). The surface of biochar was still rough and particles were remained on the biochar surface. Therefore, HAP-BC was stable even after five cycles of reuse which is consistent with the high uptake percentages after the cycles.

4. Conclusions

A novel hydroxyapatite-biochar nanocomposite was successfully synthesized and used for Pb(II), Cu(II), and Zn(II) removal in both single and ternary mixed solutions. The HAP-BC nanocomposite showed enhanced sorption, especially for Pb(II). The isotherm studies of HAP-BC indicated that Pb(II) adsorption followed the Langmuir model, while the other two ions followed the Freundlich model in both single and ternary systems. All adsorption processes were well-described by pseudo-second-order kinetics. In addition, the adsorbed HAP-BC could be recycled using HCl solution. Since HAP is an environmentally friendly material, the hydroxyapatite-biochar nanocomposites developed in this work could be an eco-friendly and low-cost adsorbent for heavy metals removal from wastewater.

Acknowledgements

This work was supported by Key research and development projects in Zhejiang Province (2015C03020), Natural Science Foundation of Zhejiang (LQ17D020002, LY16D010004), and Zhejiang Provincial Collaborative Innovation Center of Agricultural Biological Resources Biochemical Manufacturing/Zhejiang Provincial Key Lab for Chem & Bio Processing Technology of Farm Product open fund (2016KF0116).

Appendix A. Supporting information

Supplementary data associated with this article can be found in the online version at doi:10.1016/j.jssc.2018.02.010.

References

[1] K.P. Cantor, Drinking water and cancer, Cancer Causes Control 8 (1997) 292–308.
[2] P.K. Tapaswi, M.S. Moorthy, S.S. Park, C.S. Ha, Fast, selective adsorption of Cu^{2+} from aqueous mixed metal ions solution using 1,4,7-triazacyclononane modified SBA-15 silica adsorbent (SBA-TACN), J. Solid State Chem. 211 (2014) 191–199.
[3] L.F.O. Silva, C.H. Sampaio, A. Guedes, S. Fdez-Ortiz de Vallejuelo, J.M. Madariaga, Multianalytical approaches to the characterisation of minerals associated with coals and the diagnosis of their potential risk by using combined instrumental micro-spectroscopic techniques and thermodynamic speciation, Fuel 94 (2012) 52–63.
[4] H.W. Mielke, C.R. Gonzales, M.K. Smith, P.W. Mielke, Quantities and associations of lead, zinc, cadmium, manganese, chromium, nickel, vanadium, and copper in fresh Mississippi delta alluvium and New Orleans alluvial soils, Sci. Total Environ. 246 (2000) 249–259.
[5] J.C. Zwonitzer, G.M. Pierzynski, G.M. Hettiarachchi, Effects of phosphorus additions on lead, cadmium, and zinc bioavailabilities in a metal-contaminated soil, Water Air Soil Pollut. 143 (2003) 193–209.
[6] P.P. Deprez, M. Arens, H. Locher, Identification and assessment of contaminated sites at Casey Station, Wilkes Land, Antarctica, Polar Rec. 35 (1999) 299–316.
[7] A. Anjum, C. Seth, M. Datta, Removal of As^{3+} using chitosan-montmorillonite composite: sorptive equilibrium and kinetics, Adsorpt. Sci. Technol. 31 (2013) 303–324.
[8] M. Uchimiya, S. Chang, K.T. Klasson, Screening biochars for heavy metal retention in soil: role of oxygen functional groups, J. Hazard. Mater. 190 (2011) 432–441.
[9] A.W. Zularisam, A.F. Ismail, R. Salim, Behaviours of natural organic matter in membrane filtration for surface water treatment - a review, Desalination 194 (2006) 211–231.
[10] F. Fu, Q. Wang, Removal of heavy metal ions from wastewaters: a review, J. Environ. Manag. 92 (2011) 407–418.
[11] Y. Zhu, J. Hu, J. Wang, Competitive adsorption of Pb(II), Cu(II) and Zn(II) onto xanthate-modified magnetic chitosan, J. Hazard. Mater. 221–222 (2012) 155–161.
[12] T.A. Kurniawan, G.Y.S. Chan, W.H. Lo, S. Babel, Comparison of low-cost adsorbents for treating waste waters laden with heavy metals, Sci. Total Environ. 366 (2006) 409–426.
[13] X.M. Gao, Y. Zhang, Y. Dai, F. Fu, High-performance magnetic carbon materials in dye removal from aqueous solutions, J. Solid State Chem. 239 (2016) 265–273.
[14] C. Ding, W. Cheng, X. Wang, Z.Y. Wu, Y. Sun, C. Chen, X. Wang, S.H. Yu, Competitive sorption of Pb(II), Cu(II) and Ni(II) on carbonaceous nanofibers: a spectroscopic and modeling approach, J. Hazard. Mater. 313 (2016) 253–261.
[15] C. Gan, Y. Liu, X. Tan, S. Wang, G. Zeng, B. Zheng, T. Li, Z. Jiang, W. Liu, Effect of porous zinc–biochar nanocomposites on Cr(VI) adsorption from aqueous solution, RSC Adv. 5 (2015) 35107–35115.
[16] D.A. Wardle, M.C. Nilsson, O. Zackrisson, Fire-derived charcoal causes loss of forest humus, Science 320 (2008) (629-629).
[17] A.R. Zimmerman, B. Gao, M.Y. Ahn, Positive and negative carbon mineralization priming effects among a variety of biochar-amended soils, Soil Biol. Biochem. 43 (2011) 1169–1179.
[18] D. Mohan, A. Sarswat, Y.S. Ok, C.U. Pittman Jr, Organic and inorganic contaminants removal from water with biochar, a renewable, low cost and sustainable adsorbent-a critical review, Bioresour. Technol. 160 (2014) 191–202.
[19] Y. Zhou, B. Gao, A.R. Zimmerman, J. Fang, Y. Sun, X. Cao, Sorption of heavy metals on chitosan-modified biochars and its biological effects, Chem. Eng. J. 231 (2013) 512–518.
[20] M. Zhang, B. Gao, Y. Yao, Y. Xue, M. Inyang, Synthesis of porous MgO-biochar nanocomposites for removal of phosphate and nitrate from aqueous solutions, Chem. Eng. J. 210 (2012) 26–32.
[21] M. Inyang, B. Gao, Y. Yao, Y. Xue, A.R. Zimmerman, P. Pullammanappallil, X. Cao, Removal of heavy metals from aqueous solution by biochars derived from anaerobically digested biomass, Bioresour. Technol. 110 (2012) 50–56.
[22] M. Zhang, B. Gao, Removal of arsenic, methylene blue, and phosphate by biochar/AlOOH nanocomposite, Chem. Eng. J. 226 (2013) 286–292.
[23] Z. Yang, C. Zhang, Adsorption/desorption behavior of protein on nanosized hydroxyapatite coatings: a quartz crystal microbalance study, Appl. Surf. Sci. 255 (2009) 4569–4574.
[24] S.D. Jiang, Q.Z. Yao, G.T. Zhou, S.Q. Fu, Fabrication of hydroxyapatite hierarchical hollow microspheres and potential application in water treatment, J. Phys. Chem. C 116 (2012) 4484–4492.
[25] S. Saoiabi, A. Gouza, H. Bouyarmane, A. Laghzizil, A. Saoiabi, Organophosphonate-modified hydroxyapatites for Zn(II) and Pb(II) adsorption in relation of their structure and surface properties, J. Environ. Chem. Eng. 4 (2016) 428–433.
[26] Y.Y. Wang, H.H. Lu, Y.X. Liu, S.M. Yang, Removal of phosphate from aqueous solution by SiO_2–biochar nanocomposites prepared by pyrolysis of vermiculite treated algal biomass, RSC Adv. 6 (2016) 83534–83546.
[27] Y.Y. Wang, H.H. Lu, Y.X. Liu, S.M. Yang, Ammonium citrate-modified biochar: an adsorbent for La(III) ionsfrom aqueous solution, Colloid Surf. A 509 (2016) 550–563.
[28] Z. Droussi, V. D'orazio, M.R. Provenzano, M. Hafidi, A. Ouatmane, Study of the biodegradation and transformation of olive-mill residues during composting using FTIR spectroscopy and differential scanning calorimetry, J. Hazard. Mater. 164 (2009) 1281–1285.
[29] X. Xiao, B. Chen, L. Zhu, Transformation, morphology, and dissolution of silicon and carbon in rice straw-derived biochars under different pyrolytic temperatures, Environ. Sci. Technol. 48 (2014) 3411–3419.
[30] C. Bellitto, F. Federici, M. Colapietro, G. Portalone, D. Caschera, X-ray single-crystal structure and magnetic properties of Fe[CH(3)PO(3))] x H(2)O: a layered

weak ferromagnet, Inorg. Chem. 41 (2002) 709–714.
[31] L. Yue, Y. Zheng, D. Jin, Spherical porous framework of calcium carbonate prepared in the presence of precursor PS–PAA as template, Microporous Mesoporous Mater. 113 (2008) 538–541.
[32] K.S.W. Sing, D.H. Everett, R.A.W. Haul, L. Moscou, R.A. Pierotti, J. Rouquerol, T. Siemieniewska, Reporting physisorption data for gas/solid systems with special reference to the determination of surface area and porosity, Pure Appl. Chem. 57 (1985) 603–619.
[33] X.F. Qu, Q.Z. Yao, G.T. Zhou, S.Q. Fu, J.L. Huang, Formation of hollow magnetite microspheres and their evolution into Durian-like architectures, J. Phys. Chem. C114 (2010) 8734–8740.
[34] J. Yu, H. Yu, B. Cheng, X. Zhao, Q. Zhang, Preparation and photocatalytic activity of mesoporous anatase TiO_2 nanofibers by a hydrothermal method, J. Photochem. Photobiol. A 182 (2006) 121–127.
[35] I. Langmuir, The adsorption of gases on plane surfaces of glass, mica and platinum, J. Am. Chem. Soc. 40 (1918) 1361–1403.
[36] H.M.F. Freundlich, Uber die adsorption in lasugen, Z. Phys. Chem. 57 (1906) 385–470.
[37] F. Cao, P. Yin, J. Zhang, H. Chen, R. Qu, Nanoplates of cobalt phosphonate with two-dimensional structure and its competitive adsorption of Pb(II) and Hg(II) ions from aqueous solutions, J. Ind. Eng. Chem. 20 (2014) 2568–2573.
[38] L. Xiong, C. Chen, Q. Chen, J. Ni, Adsorption of Pb(II) and Cd(II) from aqueous solutions using titanate nanotubes prepared via hydrothermal method, J. Hazard. Mater. 189 (2011) 741–748.
[39] D. Wang, W. Zhang, X. Hao, D. Zhou, Transport of biochar particles in saturated granular media: effects of pyrolysis temperature and particle size, Environ. Sci. Technol. 47 (2013) 821–828.
[40] W. Cheng, S.G. Wang, L. Lu, W.X. Gong, X.W. Liu, B.Y. Gao, H.Y. Zhang, Removal of malachite green (MG) from aqueous solutions by native and heat-treated anaerobic granular sludge, Biochem. Eng. J. 39 (2008) 538–546.
[41] H. Liu, C. Wang, J. Liu, B. Wang, H. Sun, Competitive adsorption of Cd(II), Zn(II) and Ni(II) from their binary and ternary acidic systems using tourmaline, J. Environ. Manag. 128 (2013) 727–734.
[42] A.H. Chen, S.C. Liu, C.Y. Chen, C.Y. Chen, Comparative adsorption of Cu(II) Zn(II), and Pb(II) ions in aqueous solution on the crosslinked chitosan with epichlorohydrin, J. Hazard. Mater. 154 (2008) 184–191.
[43] T. Depci, A.R. Kul, Y. Önal, Competitive adsorption of lead and zinc from aqueous solution on activated carbon prepared from Van apple pulp: study in single- and multi-solute systems, Chem. Eng. J. 200–202 (2012) 224–236.
[44] A.R. Kennedy, J.B.A. Kirkhouse, K.M. McCarney, O. Puissegur, W.E. Smith, E. Staunton, S.J. Teat, J.C. Cherryman, R. James, Supramolecular motifs in s-blockmetal-bound sulfonated monoazo dyes, part 1: structural class controlled bycation type and modulated by sulfonate aryl ring position, Chemistry 10 (2004) 4606–4615.